ADVANCED HEALTHCARE MATERIALS
www.advhealthmat.de

High-Performance Artificial Ligament Made from Helical Polyester Fibers Wrapped with Aligned Carbon Nanotube Sheets

Liyuan Wang, Hongyu Jiang, Fang Wan, Hongji Sun, Yiqing Yang, Wenjun Li, Zheyan Qian, Xuemei Sun, Peining Chen,* Shiyi Chen, and Huisheng Peng**

Repairing high-load connective tissues, such as ligaments, by surgically implanting artificial grafts after injury is challenging because they lack biointegration with host bones for stable interfaces. Herein, a high-performance helical composite fiber (HCF) ligament by wrapping aligned carbon nanotube (CNT) sheets around polyester fibers is proposed. Anterior cruciate ligament (ACL) reconstruction surgery shows that HCF grafts could induce effective bone regeneration, thus allowing the narrowing of bone tunnel defects. Such repair of the bone tunnel is in strong contrast to the tunnel enlargement of more than 50% for commercial artificial ligaments made from bare polyester fibers. Rats reconstructed with this HCF ligament show normal jumping, walking, and running without limping. This work allows bone regeneration in vivo through a one-step surgery without seeding cells or transforming growth factors, thereby opening an avenue for high-performance artificial tissues.

1. Introduction

Connective tissues are the major types of tissue that transmit tensile forces and enable connective flexibility, body locomotion, and joint stability.[1] Native ligaments generally tear and rupture under high loads during vigorous activities because collagen fiber bundles stretch to the limit.[2] Approximately 200000 anterior cruciate ligament (ACL) reconstructions are performed annually in the USA.[3] Currently, biological grafts, such as autografts and allografts, are mainly used in ACL surgeries because they are intrinsically bioactive and promote new tissue growth.[3a,4] However, biological grafts are generally scarce and pose potential risks, including disease transmission and tissue rejection.[5] Therefore, developing artificial synthetic ligament grafts that are mechanically robust and integrate well with the host bone is critical.[6]

Polymeric grafts, such as poly(ethylene terephthalate) (PET), were designed to replace biological grafts in clinical trials because of their abundance, high chemical stability, and high mechanical strength.[7] However, the clinical applications of these polymeric grafts are largely limited by their intrinsically bioinert properties and poor capacity to induce new bone growth in vivo; therefore, these grafts must be fixed by interference screws at the ends of the tibial and femoral tunnels in typical ACL reconstruction surgery, easily leading to bone tunnel enlargement and long-term implant failure.[8] Although seeding transforming growth factors/cells onto these artificial grafts can enhance osteointegration to a certain extent, it can cause inevitable biological effects such as inflammation.[9] A gap exists in creating high-performance grafts with superior biomechanical robustness and bioactivity for strong integration between soft grafts and hard bones.

A native ligament is typically assembled with an anisotropic structure.[10] Briefly, nanometer-sized collagen fibrils, the basic constitutional units, are organized into micrometer-sized collagen fibers and assembled into ligaments. The nanometer channels among collagen fibrils and micrometer channels among collagen fibers provide a favorable environment for promoting new bone regeneration.[11] It has been proven that the design of channel topological structures using bare carbon nanotube (CNT) fibers indeed encourages osteointegration in vivo,[12] but the fabrication of CNT fibers is expensive and very complex. If the multilevel channel structures are introduced onto commercially available polyester fibers with excellent mechanical performance and low cost, cell proliferation and new tissue growth may occur for effective biological integration.

L. Wang, H. Jiang, H. Sun, Y. Yang, W. Li, Z. Qian, X. Sun, P. Chen, H. Peng
State Key Laboratory of Molecular Engineering of Polymers
Department of Macromolecular Science
Institute of Fiber Materials and Devices
and Laboratory of Advanced Materials
Fudan University
Shanghai 200438, China
E-mail: sunxm@fudan.edu.cn; peiningc@fudan.edu.cn; penghs@fudan.edu.cn

F. Wan, S. Chen
Department of Orthopedic Sports Medicine
Huashan Hospital
The Sports Medicine Institute
Fudan University
Shanghai 200433, China

The ORCID identification number(s) for the author(s) of this article can be found under https://doi.org/10.1002/adhm.202301610

DOI: 10.1002/adhm.202301610

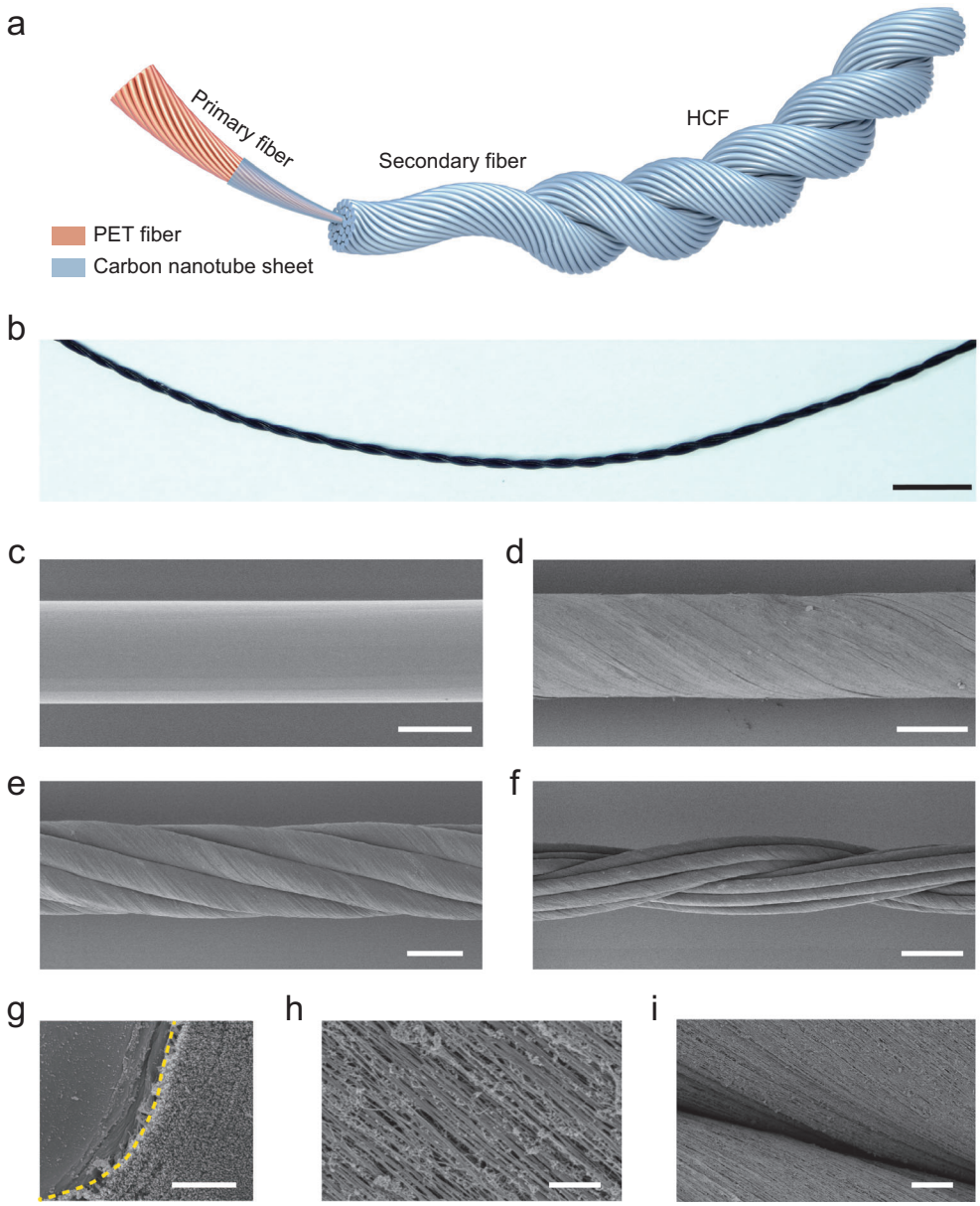

Figure 1. Core/sheath PET/CNT composite fibers assembled into helical composite fibers (HCFs) to mimic the hierarchical structure of the native ligament. a) Schematic illustration of HCFs with hierarchical helical structure. b) Photograph of an HCF. Scale bar, 5 mm. c) SEM image of a PET fiber. Scale bar, 10 μm. d) SEM image of a primary composite fiber through uniformly wrapping CNT sheets on the PET fibers. Scale bar, 100 μm. e) SEM image of a secondary composite fiber through twisting multiple primary fibers. Scale bar, 200 μm. f) SEM image of an HCF ligament through twisting multiple secondary fibers. Scale bar, 500 μm. g) SEM image of a cross-section of primary composite fiber. Scale bar, 2 μm. h) Enlarged view of the CNT sheets to show abundant nanometer-sized channels. Scale bar, 1 μm. i) Enlarged view of a secondary composite fiber to show abundant micrometer-sized channels constructed among primary fibers. Scale bar, 5 μm.

Herein, we present a high-performance and low-cost artificial ligament using aligned CNT sheets wrapped on helical PET fibers. The aligned CNT sheets and helical organization endowed these artificial ligaments with anisotropic channel structures at the nanometer and micrometer scale (**Figure 1**a). After implantation in vivo, these grafts encouraged bone regeneration and repair of bone tunnels in rats and eventually allowed the animals to stand, walk, and run with a normal gait. We demonstrated that these ligaments could promote new bone regeneration and efficient repair of the bone tunnel. These ligaments could also be continuously produced for further clinical applications.

2. Results and Discussion

In a typical preparation of helical composite fibers (HCFs), the primary building fibers were obtained by uniformly wrapping CNT sheets on the PET fibers with a diameter of ≈120 μm (Figure 1c,d,g and Figure S2, Supporting Information). CNT

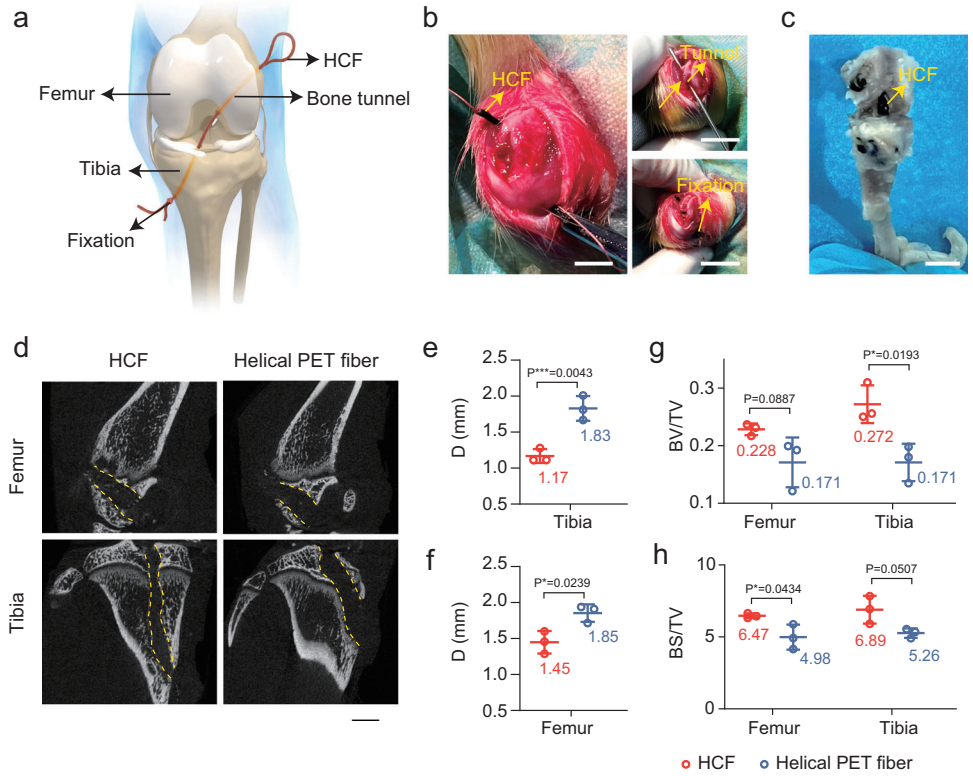

Figure 2. ACL reconstruction in rats using HCFs as artificial ligaments. a) Schematic illustration of ACL reconstruction surgery with HCFs as an artificial ligament. b) Photographs of ACL reconstruction surgery with HCFs as an artificial ligament. The bone tunnels (diameters of 1.20 mm) are drilled in the femur and tibia (right, top). The HCF graft (a diameter of 0.78 mm) is implanted through bone tunnels (left) and fixed on the host bone (right, bottom). Scale bars, 5 mm (left), 1 cm (right, top), 1 cm (right, bottom). c) Photograph of a femur-graft-tibia complex containing HCFs after implantation of 2 weeks. Scale bar, 3 mm. d) μCT images of femoral tunnel (top row) and tibial tunnel (bottom row) scanned in a coronal plane after implantation of HCFs (left) and bare helical PET fibers (right) at week 2 ($n = 3$). The bone tunnels are indicated by the yellow dotted line. Scale bar, 2 mm. e,f) Average diameters of the tibial (e) and femoral (f) tunnels after the HCFs were implanted in rats for 2 weeks ($n = 3$). p-values: 0.0043 (e), 0.0239 (f). g,h) Average ratios of BV to TV (BV/TV) and BS to TV (BS/TV) of tibial (g) and femoral (h) tunnels after the HCFs were implanted in rats for 2 weeks ($n = 3$). p-values: 0.0887 (g, left), 0.0193 (g, right), 0.0434 (h, left), and 0.0507 (h, right). All data in this figure are expressed as mean ± s.d. Statistical significance was determined by unpaired two-tailed t-test: n.s., not significant ($p > 0.05$), *$p < 0.05$, **$p < 0.01$, and ***$p < 0.005$.

sheets with aligned nanostructures (Figure S1, Supporting Information) are biocompatible and exhibit excellent mechanical properties.[13] PET fibers, which are state-of-the-art synthetic ligaments, are widely used clinically.[8a,14] After twisting multiple primary composite fibers together, secondary helical fibers (Figure 1e) were obtained, equivalent to the collagen bundles in the native ligament. HCF grafts were successfully fabricated by further twisting and folding the secondary helical fibers (Figure 1b,f). The CNTs had typical diameters of ≈10 nm; thus, the nanometer channels were formed and exhibited dimensions mostly less than 50 nm (Figure 1h and Figure S3a, Supporting Information). The micrometer-scale channels with dimensions from 1 to 12 μm were formed after helical assembly (Figure 1e,f and Figure S3b, Supporting Information). HCFs showed a slightly lower water contact angle (97.7°) and less protein adsorption than PET fibers (water contact angle of 111.3°, Figures S4 and S5, Supporting Information).

Appropriate mechanical properties of an artificial ligament are extremely important for synchronously ensuring the stability and flexibility of joint motions. The HCFs were lightweight, with a density of 0.88 g cm^{-3}. They showed higher mechanical strength (323.91 ± 16.7 MPa) than that of autografts and other polymeric counterparts like polycaprolactone and silk fiber grafts (Table S1, Supporting Information). Moreover, the failure strain and stiffness of HCFs were similar to that of native ligaments[15a,15b] thus effectively favoring the HCFs with load-displacement behaviors like native ligaments. These fibers are sufficiently flexible to withstand various deformations including bending and twisting (Figures S7 and S8, Supporting Information). Together, these mechanical profiles make the HCFs suitable for artificial ligaments.

The biosafety and stability of the HCFs were carefully studied. After implantation in rats for 2 weeks, hematoxylin and eosin (H&E) stained images and methylene blue acid fuchsin stained images showed normal cell morphology around the HCFs (Figure S9a,c, Supporting Information), and these fibers could integrate well with the surrounding tissues. The Masson-stained images indicated no scar occurred in the HCF group (Figure S9b, Supporting Information). After implantation of HCFs in rats for 2 weeks, H&E stained images showed that no CNT fragments were observed in the organs like kidney, cardiac muscle, liver, spleen, and lungs (Figure S9d, Supporting Information). These

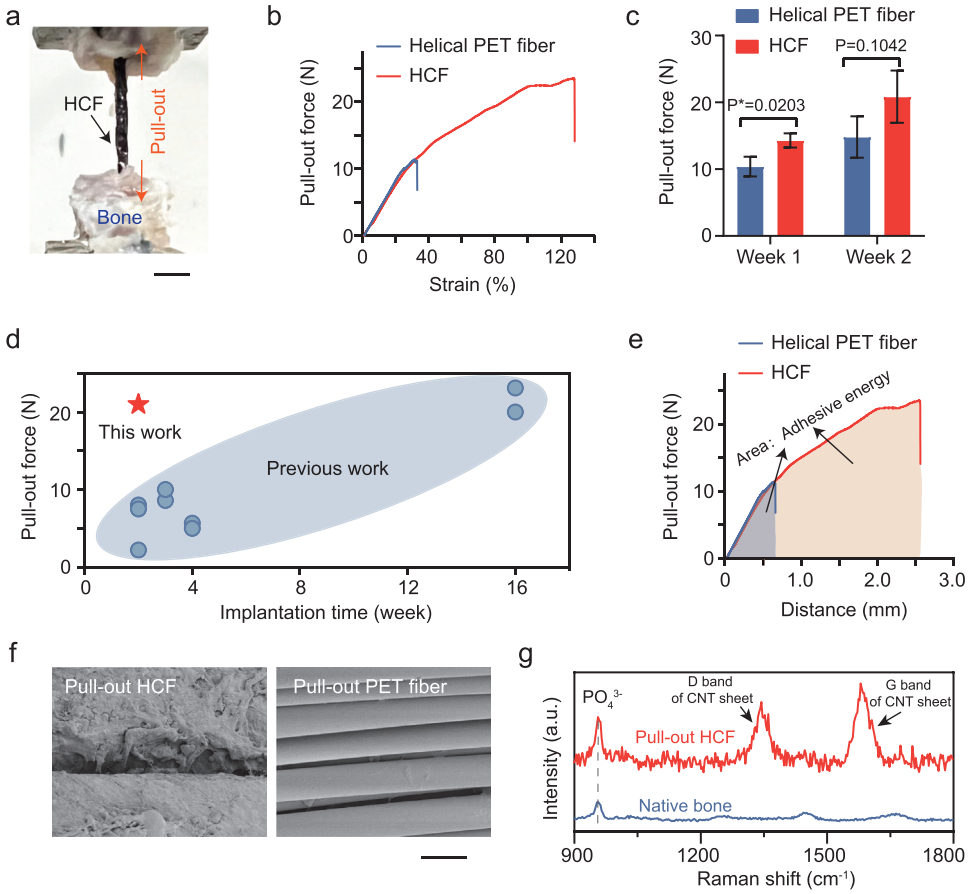

Figure 3. Pull-out test to show osteointegration induced by HCFs. a) Photograph of pull-out test, showing implanted the HCFs grafts were pulled out from the bone tunnels. Scale bar, 2 mm. b) Stress–strain curves of the pulling-out tests of the HCF and helical PET fiber grafts at week 2 ($n = 3$). c) Maximal pulling-out force of HCF and helical PET fiber grafts ($n = 3$). p-values: 0.0203 (left), 0.1042 (right). d) Comparison of the pull-out force obtained in our study with previously reported implanted ligaments. e) Adhesive energy (i.e., the area of the orange/blue area) of the HCFs and helical PET fiber grafts at week 2 ($n = 3$). f) SEM images of the pull-out HCFs and helical PET fibers at week 2. Scale bar, 30 μm. g) Raman analysis of the surface of the pull-out HCF graft at week 2. Data in (c) are expressed as mean ± s.d. Statistical significance in (c) was determined by unpaired two-tailed t-test: n.s., not significant ($p > 0.05$) and *$p < 0.05$.

results indicate that HCFs are structurally stable and biosafe in vivo.

To evaluate the osseointegration of the HCFs in vivo, we implanted these fibers into an ACL reconstruction model.[16] Following standard surgical procedures, bone tunnels (with the same diameter of 1.20 mm) were drilled into the femur and tibia. HCFs (with the same diameter of 0.78 mm) were implanted through these tunnels and fixed onto the host bone (**Figure 2**a–c). Bare helical PET fibers of the same size and helical structure were implanted as controls to compare osteointegration with that of HCFs (Figure S10, Supporting Information).

The microcomputed tomography (μCT) images showed that the tibial tunnels were not enlarged and unexpectedly narrowed by 2.5% after HCF implantation of 2 weeks (Figure 2d,e). In week 2, the CT image showed newly formed bone in the interfacial region between HCFs and native bone. Such bone regeneration was observed in femoral tunnels. By contrast, similar to previous reports, both the tibial and femoral tunnels were enlarged after the implantation of bare helical PET fibers under the same conditions. For instance, at week 2, the tibial and femoral tunnels in the bare helical PET fiber group were enlarged by 52.5% and 54.2%, respectively (Figure 2d–f), which may cause joint instability and long-term implant failure in vivo. The quantitative analysis results showed that the ratios of both bone volume to total volume (BV/TV) and bone surface to total volume (BS/TV) in the HCFs group were 1.5 times higher than those in the bare helical PET fibers at week 2 (Figure 2g,h). Moreover, for the negative controls without any supporting implanted grafts, the average diameter of bone tunnels was nearly unchanged at week 2 (Figure S11, Supporting Information). These results indicate that HCFs could strongly induce new bone growth.

The pull-out force is an important indicator for evaluating the degree of osteointegration induced by implanted grafts, which can be measured by pulling the implants out of the bone tunnels (**Figure 3**a). The implanted HCFs showed pull-out forces of 14.29 ± 1.06 and 20.85 ± 3.91 N at weeks 1 and 2, respectively, ≈1.4 times higher than that of the bare helical PET fibers (Figure 3b,c). The pull-out force for the implanted HCFs was higher than that of the reported grafts with the same implantation time (Figure 3d and Table S2, Supporting

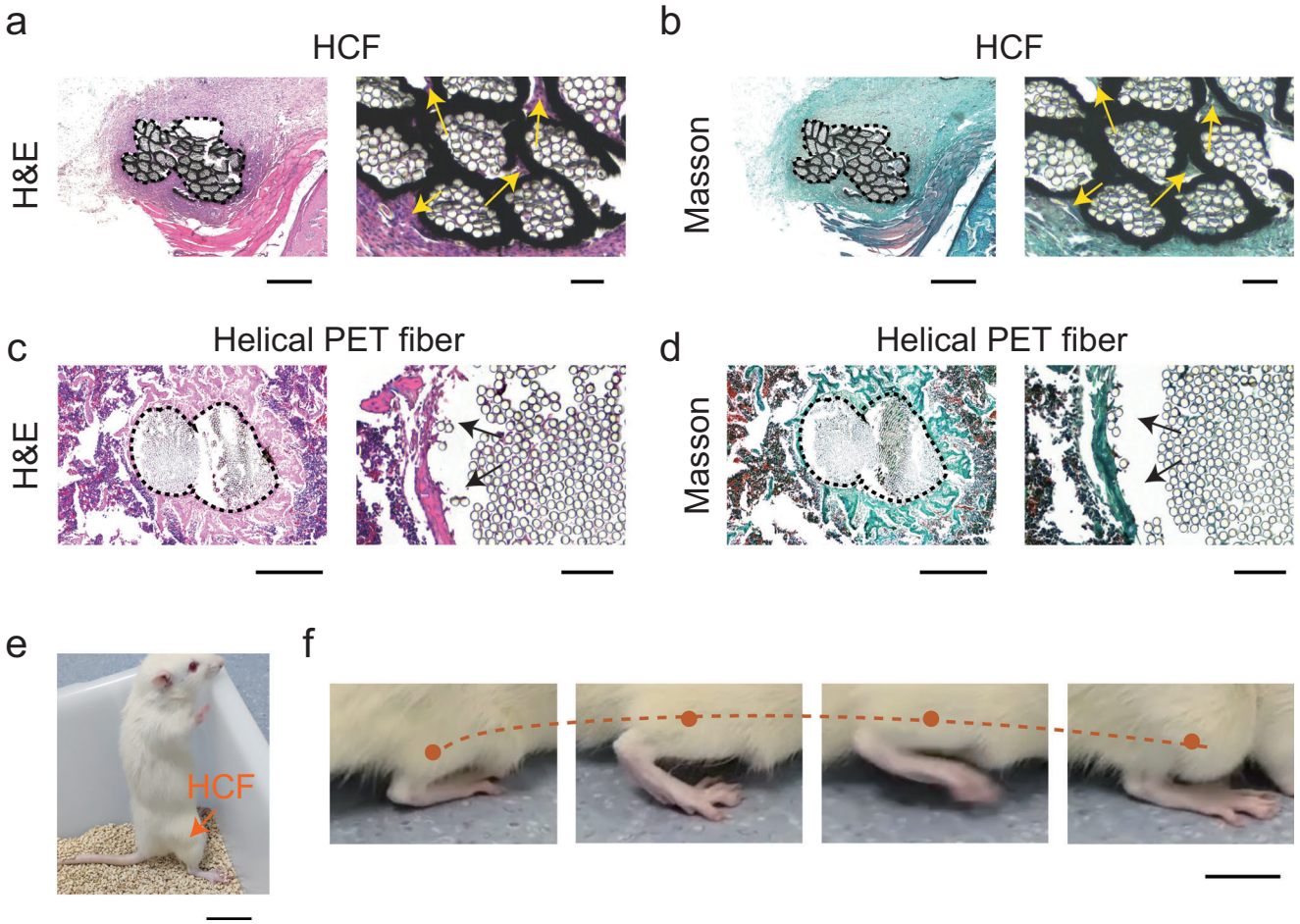

Figure 4. Histological assays and movement recovery of rats to show osteointegration of HCFs. a,b) H&E-stained images of bone tunnels implanted with HCFs (a) and helical PET fibers (b) at week 2 ($n = 3$). Newly formed bones were regenerated at the interfacial region between the HCFs and native bone, while a prominent gap was observed between the helical PET fibers and native bone. Scale bars, 500 μm (left), 100 μm (right). c,d) Masson-Goldner-stained images of bone tunnels implanted with HCFs (c) and helical PET fibers (d) at week 2 ($n = 3$). Scale bars, 500 μm (left), 100 μm (right). e) Photograph of a standing rat after reconstruction surgery of 2 weeks. Scale bar, 2 cm. f) Photographs to show the movement trail of the hindlimb, showing the rats with HCFs could successfully finish a jump. Scale bar, 1 cm.

Information), or the reported grafts needed longer implantation time to achieve pull-out forces similar to those of HCFs, indicating strong osteointegration of HCFs. The calculated adhesive energy of HCFs to the bone was nearly the same as that required for breaking the native ligament and much higher than that of bare helical PET fiber grafts (Figure 3e), demonstrating that HCFs were more osteogenic than the bare helical PET fibers. Consistent with the scanning electron microscopy (SEM) results, some newly formed bone fragments were observed on the surface of the HCFs, while little to no tissue was observed on the bare helical PET fibers (Figure 3f). Raman spectra were used to verify tissue formation during the pull-out HCF surface. The results indicated the characteristic signals of both PO_4^{3-} for calcium phosphate and D band (1344 cm^{-1}) and G band (1579 cm^{-1}) of CNT sheets could be concurrently detected (Figure 3g).

We performed histological assays to understand the biological processes underlying HCF-induced interfacial bone regeneration. Methylene blue acid fuchsin staining showed that osteoblasts were highly activated and gradually increased around the HCFs from week 1 to 2 (Figure S14, Supporting Information), indicating that HCFs could promote the activity of osteoblasts and enhance bone modeling at an early stage. H&E-stained sections revealed that newly formed bones were regenerated at the interfacial region between the HCFs and native bone at week 2. Some newly formed bones and collagen bundles started to grow in the micrometer-sized channels among the HCFs (**Figure 4**a), which was further verified by Masson-Goldner and picrosirius red-stained images (Figure 4c and Figure S15, Supporting Information). In particular, newly formed bone and collagen bundles inside HCFs could help these grafts build strong connections with the native bone. By contrast, a notable gap was observed between the bare helical PET fibers and native bone, and few newly formed bones and collagen were regenerated at both the interfacial region and inside these grafts (Figure 4b,d). Together, the histological profiles further indicated strong osteointegration of the HCF grafts. Topological structure could affect the behavior of cells by activating specific signaling pathways[12,17] such as mitogen-activated protein

kinases signaling pathway, wingless-integrated signaling pathway, and transforming growth factor-β signaling pathway. HCFs are likely to effectively induce osteointegration by activating these osteogenesis-related signaling pathways.[12]

To evaluate osseointegration in vivo, we investigated the recovery of movement in rats implanted with HCFs. In week 2, the rats were able to stand with a normal gait, and no visible bleeding or rupture occurred in the right hindlimb, even though the whole weight of the rats was pressed on their hindlimbs (Figure 4e). Eventually, the rats were able to jump, walk, and run without limping (Figure 4f and Video S1, Supporting Information).

3. Conclusion

In summary, by mimicking the hierarchical structure of the native ligament, we introduced a high-performance artificial ligament from HCFs with a PET fiber as the core and an aligned CNT sheet as the sheath. Differing from the traditional artificial ligaments, CNT sheets of these HCFs introduced unique channels at nanometer and micrometer scales, thus allowing osteointegration in vivo without seeding cells or transforming growth factors. After implantation in rats for 2 weeks, the bone tunnels were surprisingly narrowed by 2.5% in the HCF group, whereas they were enlarged by >50% in bare helical PET fibers as controls. In addition, the newly formed bone and collagen bundles could be regenerated around and inside HCFs, while a noticeable gap occurred between the bare helical PET fibers and native bone, further indicating the strong osteointegration of the HCFs. Finally, the rats implanted with HCFs could stand, walk, and run with a normal gait without limping. These novel HCF ligaments can be continuously produced on a large scale for practical applications using industrial wrapping methods. We believe that this strategy of hierarchical helical assembly can provide a new and effective solution to clinical problems associated with artificial ligaments such as bone tunnel enlargement and instability of joint movements.

4. Experimental Section

Materials Preparation: The CNT sheets utilized to wrap PET fibers (Kinetic Medical Co., Ltd.) were prepared by floating chemical vapor deposition. In this method, thiophene (1–3 wt%) and ferrocene (1–3 wt%) were used as catalysts, and ethanol (>80 wt%), toluene (3–15 wt%), Ar (100 sccm), and H_2 (1300–1600 sccm) were used as carbon source, carrier gas, and reduction gas, respectively. The reaction temperature was 1250 °C. CNT aerogel was prepared and collected into hollow socks. After densifying this CNT sock in water and ethanol, the CNT ribbon was obtained. Finally, washing this CNT ribbon with ethanol, followed by drying, the CNT sheets were successfully obtained. By using a purpose-built controllable wrapping device, the CNT sheets were wrapped on a bunch of PET fibers (with a diameter of 120 µm) using a motor, where the two ends of PET fiber were attached to two motors. The thicknesses of CNT sheets in a primary composited fiber were 10–15 µm. After twisting multi-ply CNT/PET wrapping fiber with two ends stabilized, followed by a re-twisting process after the two ends were folded together, an HCF was successfully prepared. Bare helical PET fibers with the same helical structure as HCF could also be obtained through the above twisting method. The structures of the CNT/PET wrapping fiber, HCF, and bare helical PET fiber were characterized by SEM (FE-SEM S-4800, Hitachi, Ltd.). The photographs were taken by a camera (Sony, Ltd.).

Mechanical Properties of HCF: The tensile force–displacement curves of HCFs were obtained according to the standard tensile method (Instron 5966), and the 2580 series static load cell (Catalog No. 2580–1 kN) was used in this experiment. The stiffness and modulus were calculated as the ratio of tensile force to displacement and the ratio of tensile stress to strain, respectively.

ACL Reconstruction on Rats: The SD rats (male, 8–10 weeks) were purchased from Shanghai SLAC Laboratory Animal Co., Ltd. The HCFs were implanted into rats for 1 and 2 weeks, and bare helical PET fibers as controls were implanted with the same conditions. The above fiber materials showed the same helical structure, diameter (0.78 mm), and length (3.5 cm). The ACL reconstruction surgery was performed on the right hindlimbs. Briefly, after the rats were anesthetized by isoflurane (1.5 v/v%), a medial parapatellar incision was made and disinfected with iodophors. After cutting the skin layer by layer, the native ACL was exposed and transected. The bone tunnels of the tibia and femur were created by using a Kirschner wire (a diameter of 1.20 mm). The HCF graft was pulled into these bone tunnels with an Ethibond guide wire (Ethicon), and then both ends of the graft were knotted to fix with the host bone. After suturing, all the rats were freely moving in the cages. The potassium penicillin (200 000 IU) was injected intramuscularly once a day for 5 days continuously.

Micro-Computed Tomography Tests: The rats implanted with HCFs and bare helical PET fibers were sacrificed after surgery for 1 and 2 weeks. The femur-graft-tibia complex was taken out and performed the µCT tests (SkyScan 1176, BRUKER, operated at 50 kV and 500 µA). The CTAn analysis was used to calculate the average diameter of the bone tunnel, BV/TV, and BS/TV.

Bio-Mechanical Pull-Out Tests: The mechanical tests of the femur-graft-tibia complex were performed by using an electronic universal material testing system (Instron 5569). The 2525 Series static load cell (Catalog No. 2525-806-1 kN) was used in this experiment. Both the femur and tibia were fixed with pneumatic clamps. These pull-out tests were performed with an extension rate of 2 mm min^{-1} after 1–2 N static preloading for 30 s. After the grafts were pulled out from the bone tunnels completely, the pull-out force–displacement curve and the maximum pull-out force were calculated.

Histological Examination: After these femur-graft-tibia complexes were fixed in 4% paraformaldehyde for 48 h and decalcified for 4 weeks, the histological examination was performed. These tissues were sliced into thick sections with ≈3 µm using a microtome (Leica RM 2135, Leica Microsystems). The hematoxylin, eosin-staining solution, and 0.1% picrosirius-red-staining solution (Head Biotechnology. Co., LTD, 26357–02) were used to perform H&E staining and picrosirius-red-staining, respectively. The methylene blue Solution A and B (Leagene, DB0088) were utilized to perform methylene blue-acid fuchsin staining. The Masson-Goldner-staining was performed by successively staining the slices with Goldner I (Morphisto, 25642–2), Goldner II (Morphisto, 26966–2), and Goldner III (Morphisto, 26007–11). Finally, all the images were obtained by microscopy (IX71SBF2, Olympus Corporation).

Approval Statement: All the animal experiments were approved by the Institutional Animal Care and Use Committee at Fudan University (No. SYXK2020-0032).

Statistical Analysis: Statistical analysis was performed with Graphpad Prism 9.0, Microsoft Excel 2016, Origin 2018, and Adobe Illustrator CC 2023. All the images were confirmed by at least three independent experiments. The results are expressed as mean ± s.d. of three independent experiments unless otherwise stated. The statistical differences between the two groups were analyzed using an unpaired two-tailed *t*-test. *p*-values: n.s., not significant ($p > 0.05$), $*p < 0.05$, $**p < 0.01$, $***p < 0.005$, and $****p < 0.001$.

Supporting Information

Supporting Information is available from the Wiley Online Library or from the author.

Acknowledgements

This work was supported by MOST (2022YFA1203001, 2022YFA1203002), NSFC (T2321003, 22335003, 52122310, 22075050, T2222005, 22175042, 52203256), and STCSM (21511104900, 20JC1414902), and China Postdoctoral Science Foundation (BX2021074).

Conflict of Interest

The authors declare no conflict of interest.

Author Contributions

L.W. and H.J. contributed equally to this work. L.W., H.J., and P.C. conceived and designed the experiments. X.S., P.C., and H.P. directed the project. H.J., H.S., Y.Y., and W.L. prepared the fiber materials. F.W., H.J., H.S., and L.W. conducted animal experiments. F.W., H.J., H.S., and L.W. analyzed the data. All authors reviewed and critiqued the results, and made key revisions to the manuscript.

Data Availability Statement

The data that support the findings of this study are available from the corresponding author upon reasonable request.

Keywords

artificial ligaments, carbon nanotubes, hierarchical helical fibers, osteointegration, polyester fibers

Received: May 20, 2023
Revised: September 9, 2023
Published online: September 26, 2023

[1] a) S. Camarero-Espinosa, H. Yuan, P. J. Emans, L. Moroni, *Adv. Healthcare Mater.* **2023**, *12*, 2203023; b) K. L. Moffat, W.-H. S. Sun, P. E. Pena, N. O. Chahine, S. B. Doty, G. A. Ateshian, C. T. Hung, H. H. Lu, *Proc. Natl. Acad. Sci. USA* **2008**, *105*, 7947; c) A. Nasseri, H. Khataee, A. L. Bryant, D. G. Lloyd, D. J. Saxby, *Comput. Methods Programs Biomed.* **2020**, *184*, 105098.

[2] a) C. Aka, G. Basal, *J. Mech. Behav. Biomed. Mater.* **2022**, *126*, 105063; b) F. Sheng, B. Zhang, Y. Zhang, Y. Li, R. Cheng, C. Wei, C. Ning, K. Dong, Z. L. Wang, *ACS Nano* **2022**, *16*, 10958.

[3] a) H. Yazdi, A. Moradi, A. Sanaie, A. Ghadi, *J. Orthopaed. Traumatol.* **2016**, *17*, 327; b) C. T. Laurencin, J. W. Freeman, *Biomaterials* **2005**, *26*, 7530.

[4] B. Wipfler, S. Donner, C. M. Zechmann, J. Springer, R. Siebold, H. H. Paessler, *Arthroscopy* **2011**, *27*, 653.

[5] C. R. Arciola, D. Campoccia, L. Montanaro, *Nat. Rev. Microbiol.* **2018**, *16*, 397.

[6] a) M. T. Rodrigues, R. L. Reis, M. E. Gomes, *J. Tissue Eng. Regen. Med.* **2013**, *7*, 673; b) H. Li, J. Li, J. Jiang, F. Lv, J. Chang, S. Chen, C. Wu, *Acta Biomater.* **2017**, *54*, 399.

[7] a) T. Nau, P. Lavoie, N. Duval, *J. Bone Jt. Surg., Br. Vol.* **2002**, *84*, 356; b) Y. Wu, Y. Zhang, R. Zhang, S. Chen, *Front. Bioeng. Biotech.* **2021**, *9*, 630745.

[8] a) J. Cai, F. Wan, Q. Dong, J. Jiang, C. Ai, D. Sheng, W. Jin, X. Liu, Y. Zhi, S. Wang, Y. Sun, J. Chen, Z. Shao, S. Chen, *J. Mater. Chem. B* **2018**, *6*, 5738; b) L. M. Batty, C. J. Norsworthy, N. J. Lash, J. Wasiak, A. K. Richmond, J. A. Feller, *Arthroscopy* **2015**, *31*, 957.

[9] a) C.-H. Lee, M. U. Jin, H.-M. Jung, J.-T. Lee, T.-G. Kwon, *PLoS One* **2015**, *10*, e0120051; b) X. Shen, Y. Zhang, Y. Gu, Y. Xu, Y. Liu, B. Li, L. Chen, *Biomaterials* **2016**, *106*, 205.

[10] a) C. Zhu, S. Pongkitwitoon, J. Qiu, S. Thomopoulos, Y. Xia, *Adv. Mater.* **2018**, *30*, 1707306; b) D. Docheva, S. A. Müller, M. Majewski, C. H. Evans, *Adv. Drug Delivery Rev.* **2015**, *84*, 222.

[11] a) Y. Bi, D. Ehirchiou, T. M. Kilts, C. A. Inkson, M. C. Embree, W. Sonoyama, L. Li, A. I. Leet, B.-M. Seo, L. Zhang, S. Shi, M. F. Young, *Nat. Med.* **2007**, *13*, 1219; b) V. Kishore, W. Bullock, X. Sun, W. S. Van Dyke, O. Akkus, *Biomaterials* **2012**, *33*, 2137; c) T. K. H. Teh, S.-L. Toh, J. C. H. Goh, *Tissue Eng., Part A* **2013**, *19*, 1360.

[12] L. Wang, F. Wan, Y. Xu, S. Xie, T. Zhao, F. Zhang, H. Yang, J. Zhu, J. Gao, X. Shi, C. Wang, L. Lu, Y. Yang, X. Yu, S. Chen, X. Sun, J. Ding, P. Chen, C. Ding, F. Xu, H. Yu, H. Peng, *Nat. Nanotechnol.* **2023**, *18*, 1085.

[13] a) K. Lawton, H. Le, C. Tredwin, R. D. Handy, *Int. J. Nanomed.* **2019**, *14*, 7947; b) J. Wang, C. Huang, Y. Wang, Y. Chen, Z. Ding, C. Yang, L. Chen, *Colloids Surf., A* **2020**, *606*, 125520.

[14] Z. Kang, D. Li, C. Shu, J. Du, B. Yu, Z. Qian, Z. Zhong, X. Zhang, B. Yu, Q. Huang, J. Huang, Y. Zhu, C. Yi, H. Ding, *Front. Bioeng. Biotech.* **2021**, *9*, 749221.

[15] a) D. A. Brennan, A. A. Conte, G. Kanski, S. Turkula, X. Hu, M. T. Kleiner, V. Beachley, *Adv. Healthcare Mater.* **2018**, *7*, 1701277; b) W. A. Grana, D. M. Egle, R. Mahnken, C. W. Goodhart, *Am. Sport. Med.* **1994**, *22*, 344; c) G. A. Lichtwark, A. M. Wilson, *J. Exp. Biol.* **2005**, *208*, 4715.

[16] a) Q. Dong, J. Cai, H. Wang, S. Chen, Y. Liu, J. Yao, Z. Shao, X. Chen, *Acta Biomater.* **2020**, *106*, 102; b) R. H. Brophy, D. Kovacevic, C. W. Imhauser, M. Stasiak, A. Bedi, A. J. Fox, X.-H. Deng, S. A. Rodeo, *J. Bone Jt. Surg., Am. Vol.* **2011**, *93*, 381.

[17] a) M. M. Stevens, J. H. George, *Science* **2005**, *310*, 1135; b) Y. Li, Y. Xiao, C. Liu, *Chem. Rev.* **2017**, *117*, 4376.